## Fabrication of an atom chip for Rydberg atom-metal surface interaction studies

O. Cherry,\* J. D. Carter, and J. D. D. Martin

Department of Physics and Astronomy and Institute for Quantum Computing,

University of Waterloo, Waterloo, Ontario, N2L 3G1, Canada

(Dated: October 15, 2025)

An atom chip has been fabricated for the study of interactions between <sup>87</sup>Rb Rydberg atoms and a Au surface. The chip tightly confines cold atoms by generating high magnetic field gradients using microfabricated current-carrying wires. These trapped atoms may be excited to Rydberg states at well-defined atom-surface distances. For the purpose of Rydberg atom-surface interaction studies, the chip has a thermally evaporated Au surface layer, separated from the underlying trapping wires by a planarizing polyimide dielectric. Special attention was paid to the edge roughness of the trapping wires, the planarization of the polyimide, and the grain structure of the Au surface.

PACS numbers: 85.40.Ls, 34.35.+a, 37.10.Gh, 32.80.Ee

**Note:** This is a manuscript prepared approximately 13 years ago, intended to be combined with experimental demonstration of the chip to trap atoms. The first author passed away in September 2024. The fabrication techniques may be useful to others.

### I. INTRODUCTION

A Rydberg atom has a single electron excited to a state of high principal quantum number n. Rydberg atoms are remarkable – compared to less excited atoms – for their exaggerated properties, stemming from a large average separation of their excited electron and ion-core [1]. In particular, they are highly susceptible to electric fields: their polarizabilities scale like  $n^7$ , and the field required for removal of the excited electron (ionization) scales like  $1/n^4$ .

Rydberg atoms also exhibit enhanced interactions with metal surfaces. The image charge picture is useful for understanding these interactions [2]. Energy shifts due to the interaction of the Rydberg atom with its image dipole scale like  $n^4/z^3$ , where z is the distance to the surface. This has been observed spectroscopically by Sandoghdar et al. [3]. Closer to the surface, the interaction becomes highly non-perturbative, and the Rydberg atom may be field ionized by its own image. Hill et al. [4] have experimentally verified that this occurs at an atom-surface distance of  $4.5a_0n^2$ , where  $a_0$  is the Bohr radius.

There have been two notable challenges in previous Rydberg atom surfaces experiments: 1) control and/or determination of the atom-surface distance z, and 2) minimization of the influence of stray surface electric fields. This paper describes the fabrication of an "atom chip" [5, 6] suitable for Rydberg atom-surface interaction studies at *controllable* separations. We discuss its use for characterizing stray electric fields close to surfaces.

Atom chips are based on the principle that paramagnetic atoms experience mechanical forces in inhomoge-

neous magnetic fields. In particular, atoms in low-field seeking states are drawn to regions of low magnetic field magnitude. Micron-scale current-carrying wires lithographically patterned on a substrate (known as "magnetic microtraps" or "atom chips") can be used to produce local magnetic field minima [5, 6]). These chips can trap translationally cold atoms obtained from laser and evaporative cooling at variable distances from their surfaces. The distance from the surface may be varied by changing the currents in the wires generating the potentials. For example, atom chips have been used to observe the Casimir-Polder force between ground-state atoms and dielectric surfaces – this force reduces the well-depth for the trapped atoms, causing increased atom loss as the surface is approached [7].

Initial work on Rydberg excitation using atom chips near surfaces has shown large inhomogeneous fields due to adsorbed Rb [8]. However, even without adsorbed contaminants we expect to observe inhomogeneous patch fields due to the polycrystalline nature of the metal surface. We plan to measure these "patch fields" as a function of distance from the surface by exciting magnetically microtrapped atoms. The spectral broadening of these transitions will indicate the patch field magnitudes. We have designed and fabricated an atom chip for this purpose.

## II. DESIGN

In this section we discuss the design rationale for the atom-chip. Use of the chip for Rydberg atom-surface experiments requires: a source of cold atoms, the capability to load them into the trap, and equipment for the excitation and detection of Rydberg atoms. These aspects of the experiment are discussed in Appendix A.

There are five parallel trapping wires at the center of the chip (see Fig. 1a). These are approximately 4 mm long. The center wire is 7  $\mu$ m wide, sufficiently narrow to form a tight trap close to the wire. It is an H-shaped wire, allowing it to function as either a Z- or U-wire (C<sub>1-4</sub>). A 7  $\mu$ m wide U-shaped wire sits on either side of the

<sup>\*</sup> Deceased.

center wire, separated from the center wire by a  $7 \mu m$  gap  $(UI_{1-2}, UI_{3-4})$ . A  $14 \mu m$  wide U-wire neighbors each of the inner U-wires  $(UO_{1-2}, UO_{3-4})$ , separated by  $300 \mu m$  (see Fig. 1b). Each wires terminates in a bond pad at the edge of the chip.

To load the chip, will form a trap far away from the chip surface  $(z>200\,\mu\mathrm{m})$ , by running currents in the same direction in the center wire and inner U-wire, and flowing in the opposite direction in the outer U-wire. For traps at intermediate distances  $(50< z<200\,\mu\mathrm{m})$  the center wire and outer U-wire will have currents flowing in opposite directions (and the inner U-wire not used). Close to the chip  $(z<50\,\mu\mathrm{m})$  traps will be created with the center wire current opposing the current in the inner U-wire (and the outer U-wire not used).

The atom chip allows precise control of the atom surface distance. However, there is some uncertainty in this distance due to the finite size of the trapped atom cloud. This is detailed in Appendix B.

The current-carrying wires responsible for magnetic trapping will have appreciable voltage drops along their lengths and voltage differences between them. If unshielded, these would create strong electric field inhomogeneities over the trapped atom sample. As Rydberg atoms are especially sensitive to electric fields, this is undesirable. In addition, exposed dielectric between the wires may charge up, creating time dependent electric fields. To avoid these problems it is necessary to have a "shield layer" between the wires and the atoms. To prevent charging, this shield should be conductive (a metal or doped semiconductor), but insulated from the trapping wires below. For mechanical rigidity and durability it makes sense to use an insulating dielectric layer. However, this layer should not be too thick, as it will increase the distance between the trapping wires and atoms, reducing the trap confinement. The trap should be as confining as possible, so that the atom-surface distance is well-defined.

It is also desirable for the insulating layer to "planarize" the underlying wire topography. The shield layer should be as flat as possible, presenting an idealized surface to the atoms, which will facilitate comparison with theory. For this reason we will refer to the intermediate, insulating layer between the wires and shield as the "planarization layer".

A flat, reflective surface is often required above an atom chip to form a mirror MOT [9]. For example, Reichel et al. [10] have used a replica transfer technique. A chip was covered in epoxy, and then a flat substrate with a thin silver layer (a mirror) was placed face down on the chip, separated from its surface by spacers. Once the epoxy cured, the substrate was lifted off, leaving a flat silver layer on top of the chip. The epoxy layer was approximately  $25\,\mu\mathrm{m}$  thick – which significantly reduces the confinement possible near the chip surface. However, it is possible that modifications of this approach could produce thinner planarization layers.

An improvement to these methods is to coat the wires

with a planarizing dielectric polymer. Both polyimide and benzo-cyclo-butene (BCB) have been used to obtain flatter surfaces [11], [12], [13], [14]. Their application and patterning are compatible with standard clean room practices and fabrication equipment. In this work we chose to use polyimide PI 2562 from HD Microsystems, with a single-layer thickness of  $1.4\,\mu\mathrm{m}$  when spun at 3000 RPM. Additional layers can be deposited either before or after curing the film.

The planarization requirement may be lessened by submerging the trap wires in the substrate [12]. This has the additional advantage of improving thermal conduction from the wires. A possible limitation of this technique is the edge roughness of the wires. Despite the additional processing required, this approach is worth further investigation.

As Rydberg atoms will directly interact with the shield, its properties are important. Gold was chosen for its chemical inertness and ease of thermal evaporation. As was mentioned in the Introduction, a major challenge in Rydberg atom experiments are the stray electric fields produced by the surface. These may have several origins. As discussed in Appendix C, so-called "patch fields" are produced by polycrystalline surfaces typical of thermal evaporation of thin gold films. To minimize these patch fields it is desirable to minimize grain size. This can be influenced to some degree by the evaporation conditions and film thickness, as we shall discuss later.

## III. FABRICATION

The substrate used in our atom chip fabrication is Si with a 40 nm thermally-grown  $\mathrm{SiO}_2$ , which insulates electrically, and has been shown to be thin enough to provide sufficient thermal contact to the substrate [15]. Before patterning, wafers are cleaned using the RCA 1 process (5:1:1  $\mathrm{H}_2\mathrm{O}:\mathrm{NH}_4\mathrm{OH}:\mathrm{H}_2\mathrm{O}_2$  [16]) to remove unwanted organic contamination that may have occurred during storage.

The dimensions of the chip are  $2.02 \times 2.02 \,\mathrm{cm}$  – constrained to the largest size that will fit through a 2.75 in Conflat port on the vacuum chamber.

The wires are patterned using AZ 2035 nLOF negative photoresist spun at 2000 RPM to give a thickness after baking of between 3.5 and  $4.0\,\mu\text{m}$ . The resist process follows the recommendations of the manufacturer [17] except developing time is increased to 120 s to increase undercut into the sidewalls.

Metal films (for both the wires and surface shield) are deposited using an Edwards E306A thermal deposition system. The system uses a diffusion pump to reach a base pressure of between  $7 \times 10^{-7}$  and  $3 \times 10^{-6}$  Torr. Film thickness is monitored using a 6 MHz quartz crystal oscillator. For reasons discussed later, we use a Ti/Pd/Au adhesion layer for the wires, and a Cr/Au adhesion layer for the shield. We evaporate Cr from a tungsten rod electroplated with a thick layer of Cr. Ti is evaporated from

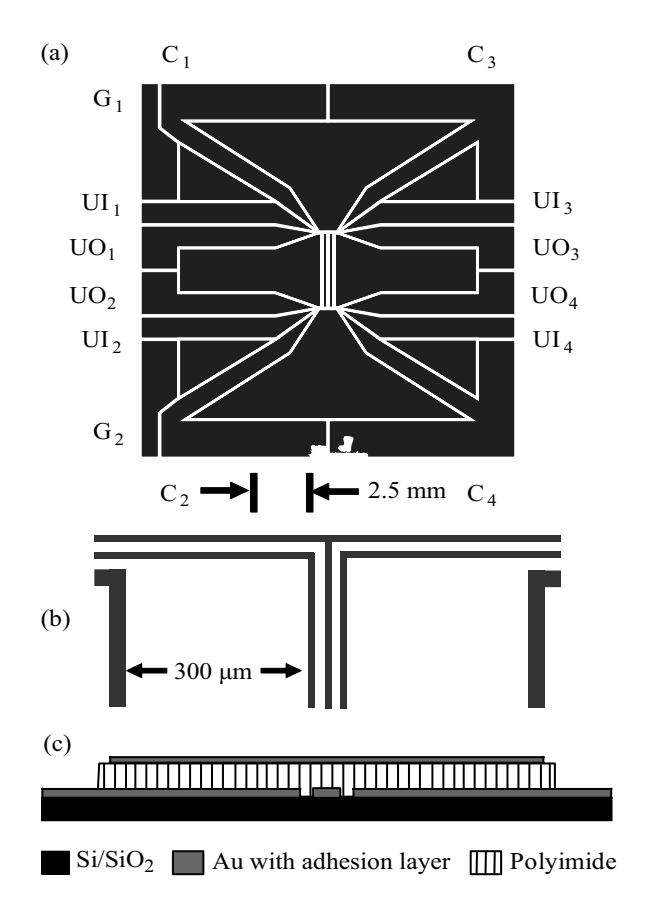


FIG. 1. Schematic of the atom chip. (a) Trapping wires (b) Magnified view of the end of the center wire strip is shown at right. The widths of the center wires and spaces are  $7 \mu m$ , but are exaggerated here for clarity. (c) Cross section of the chip.

a cylindrical pellet sitting in a tungsten boat. Pd is evaporated from cylindrical pellets with a tungsten coil and alumina crucible. The source of Au is a 1 Oz bar cut into small pieces. Au is evaporated in an alumina crucible heated by a tungsten coil. In order to minimize radiative heating which may damage the resist, the substrate mount is water cooled.

The corresponding remover for AZ 2035 nLOF resist is AZ Kwik Strip. However, the first stage of lift-off is in warm acetone. Hot Kwik Strip is then used to remove baked-on resist residue. A low power ultrasonic clean in isopropanol removes metal flakes that may have clung to the surface.

The chip is planarized using PI 2562 polyimide. An adhesion promoter, VM 652, is first spun over the chip at 3000 RPM and baked on a hotplate at 120 °C for 30 s. A 2 cm disk of PI 2562 is poured onto the chip and spun at 500 RPM for 10 s followed by 3000 RPM for 30 s. It is baked immediately after spinning at 120 °C for 5 min. The polyimide is cured in a nitrogen fed furnace at 200 °C for 30 min and 350 °C for 60 min with ramps of 4 °C/min and 2.5 °C/min ramps, respectively. A single layer of cured PI 2562 has a thickness of  $1.3-1.5\,\mu\mathrm{m}$ . To in-

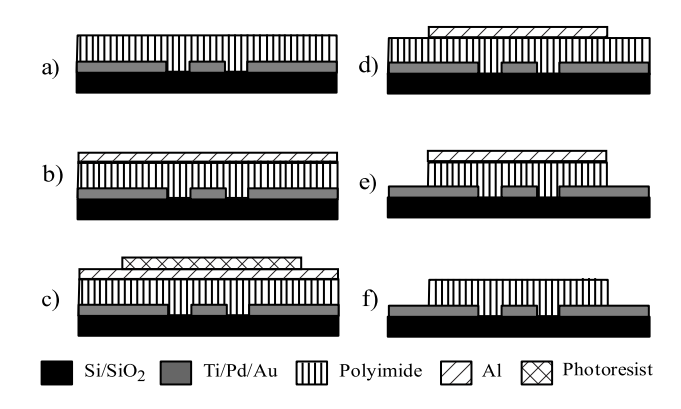


FIG. 2. Patterning of polyimide planarization layer: a) coat and cure polyimide; b) sputter Al; c) pattern positive photoresist over Al; d) wet etch Al using photoresist as mask, then remove photoresist; e) reactive ion etch (RIE) polyimide using Al as mask; f) wet etch to remove remove Al mask.

crease planarization, the chip is coated with two additional layers of polyimide, with a full cure between each. Multiple layers of PI 2562 may be coated before curing, but this has been found to result in a lower degree of planarization.

The polyimide must be removed around the perimeter of the chip to reveal the bond pads of the underlying wires. The polyimide is patterned using ICP-RIE (Trion Phantom II) with  $O_2$  as the etch gas. The patterning process is shown in Fig. 2. A sputtered Al layer,  $0.5-1\,\mu\rm m$  thick, acts as the etch mask. It is patterned using AZ 3312 positive photoresist and etched in PAN etch (1:16:1:2 H<sub>3</sub>PO<sub>4</sub>:CH<sub>3</sub>COOH:HNO<sub>3</sub>:HNO<sub>3</sub>:H<sub>2</sub>O) at 40 – 45 °C. The polyimide is etched in ICP/RIE at a pressure of 10 mTorr and an  $O_2$  flow rate of 35 sccm. An ICP power of 500 W and a RIE power of 25 W gives an etch rate of about  $0.85\,\mu\rm m/min$ . After the etch, the Al is removed in PAN.

In order to avoid etching unwanted pinholes through the polyimide, coating and etching is performed twice. The chip is first coated with two layers of polyimide (with a cure after each coating) which are then etched. The chip is then coated with a third layer of polyimide which is patterned using the same process as the first two. Since the depth of this second etch is less than that of the first, a hole cannot be etched through all three layers.

The shield layer is deposited using thermal evaporation and patterned with lift-off lithography using the same process as the wires. The Au thickness is  $100 \,\mathrm{nm}$  with a  $12-20 \,\mathrm{nm}$  Cr adhesion layer. The shield is connected to ground pads  $G_1$  and  $G_2$  (see Fig. 1a) using small drops of Epotek H21D silver-filled epoxy.

The chip is mounted on a machined Macor block using Epotek 353ND epoxy. Electrical connections between the chip and Au pads on the mount are made using ultrasonic wedge bonding with  $25 \times 250 \,\mu\mathrm{m}$  Au ribbon. Each connection uses two ribbons to reduce the current passing through a ribbon, and to add security in case a ribbon breaks or a bond becomes unstuck. The strength of each

bond is enhanced with a bead of Epotek H21D epoxy.

#### IV. RESULTS

Several measurements and tests of the chip have been made to ensure that it will perform satisfactorily. Wire heating has been measured to be very similar to the measured values of chips fabricated by Groth  $et\ al.$  [15] both at fast timescales (dependent on the contact resistance between the wires and substrate) and slow timescales (dependent on the thermal conductivity of the substrate). In air, the chip can support current densities of above  $9\times 10^6\ {\rm A/cm^2}$  with a 500 ms pulse length and is expected to perform similarly under vacuum.

As was mentioned in the previous section we use Ti as an adhesion layer with a Pd intermediate diffusion barrier for the Au wires. We have measured interdiffusion effects for various metallizations. The trapping wires of early chips were fabricated using Cr as the adhesion layer. It was observed that, after the subsequent high temperature processing of the polyimide layer, the resistance in the wires increased by over 120% due to interdiffusion between the Cr and Au. This effect was very similar to that measured by Madakson [18] and Munitz et al. [19] who showed that resistance increases as the Cr diffuses into the gold film through grain boundaries at temperatures above 300 °C. Once it reaches the surface it forms an oxide, Cr<sub>2</sub>O<sub>3</sub>. The resistance reaches a maximum as Cr saturates the Au film and then drops off once the Cr layer becomes depleted. Eventually the majority of Cr is converted to  $Cr_2O_3$  and the resistivity decreases. The measurement of this chip indicated that, after three polyimide cure processes, resistance had reached the saturation point, and that the Cr adhesion layer was not yet depleted. As a test, chips were also fabricated using Ti/Au and Cr/Pd/Au metallizations. Figure 3 plots the increase in wire resistance after successive cure cycles for each metallization. As it can be seen the Cr/Au and Cr/Pd/Au metallizations exhibited the poorest performance with resistance increasing by over 125% and 55% respectively. The resistance of the Ti/Au wires increased by 0.5% and the Ti/Pd/Au wire resistance decreased by approximately 1%.

Another concern with diffusion is the buildup of oxide on the wire surface. This causes problems when making electrical connections by wirebonding. The ability to make reliable, adherent bonds on Cr/Au bond pads with gold ribbon was found to decrease significantly after a 400 °C bake by Pan et al. [20]. Our attempts to wirebond to the Cr/Au contacts after curing meet with the same problems. The wires can be easily pulled from the surface even if they appear to stick after making the bond. In contrast, bondability to Ti/Pd/Au chips is excellent.

The edge roughness of a typical wire is shown in Fig. 4 . This chip has been submitted to three cures at  $350\,^\circ\mathrm{C}$ , which has had an annealing effect on the metal. Before curing, the wire edge roughness is limited to deviations

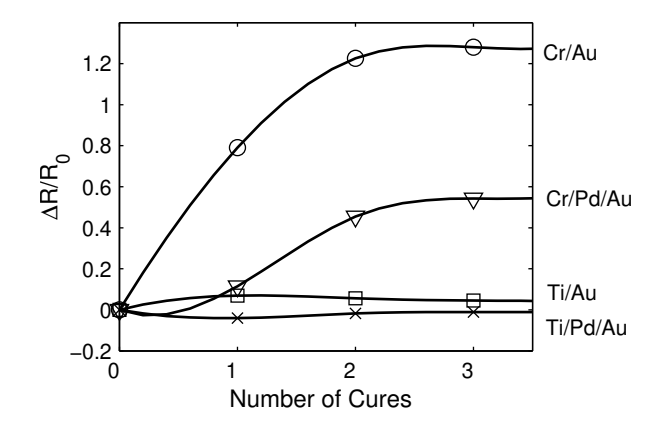


FIG. 3. Change in resistance in the center wire with  $\rm Cr/Au$ ,  $\rm Ti/Au$ ,  $\rm Cr/Pd/Au$  and  $\rm Ti/Pd/Au$  metallizations after subjecting to polyimide cure cycles. The solid lines are to aid the eve

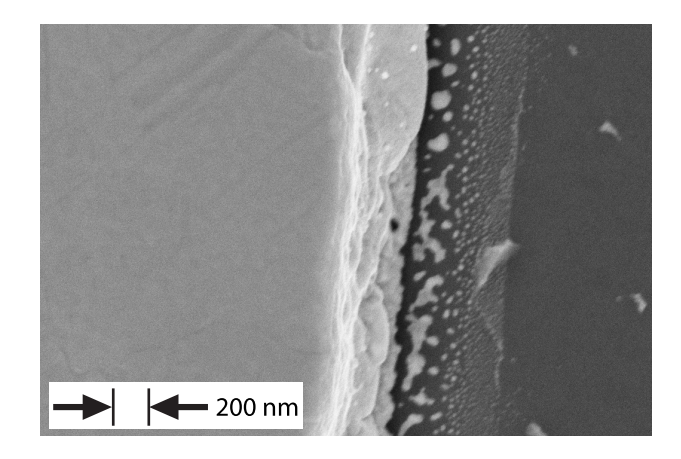
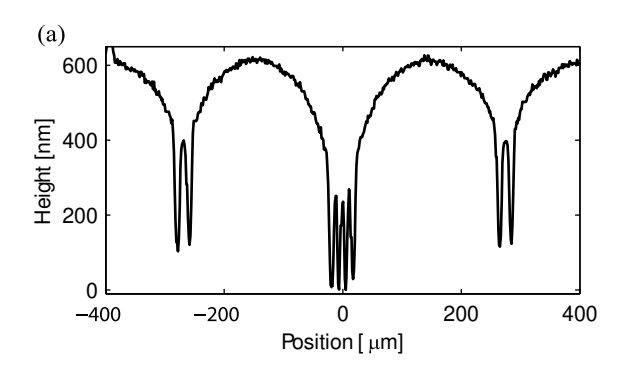


FIG. 4. SEM image of a wire edge. To the right of the wire is a thin layer of metal that reached the wafer at a non-normal incident angle and passed beneath the undercut of the photoresist. This film exists exhibits the characteristics of island formation in preliminary thin film growth [21].

of about 100 nm by the edges of the photoresist. After curing, the wire edge features are instead limited by the larger grain size of the annealed Au. The grains have grown from the pre-annealed size of  $50-100\,\mathrm{nm}$  to between 3 and  $10\,\mu\mathrm{m}$ . Despite the enlarged grain size, the edge deviations have only increased to about 200 nm.

The degree of planarization (DOP) of a film is defined as DOP =  $[1 - \Delta h/h_w] \times 100\%$ , where  $\Delta h$  is the deviation in the surface topography, and  $h_w$  is the height of the underlying features. A single layer of PI 2562, spun at 3000 RPM, to a thickness of 1.4  $\mu$ m gives a 40% DOP over the center wire. Coating with two layers of PI 2562 before curing increases DOP to 50-60%. In contrast applying a layer of PI 2562 over a fully-cured single layer gives a DOP of 70-80%. Planarization is improved further to 80-90% by applying a third layer. As a demonstration of the planarization, a region of polyimide over



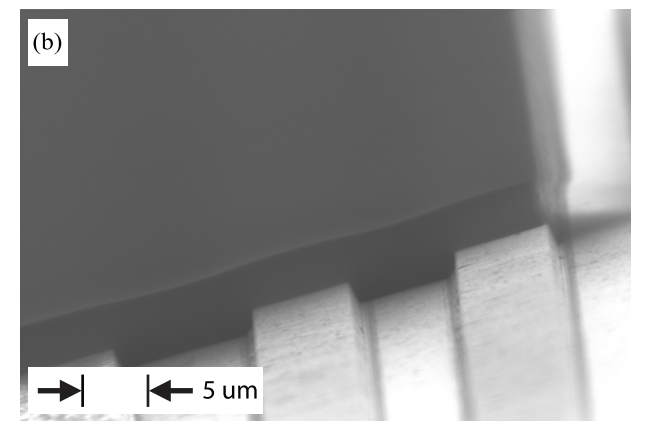


FIG. 5. (a) Stylus profilometer (Dektak) scan of polyimide surface over the five center wires. Polyimide was coated in three layers with full cure between each. (b) SEM image of an etched polyimide film demonstrating the extent of planarization over the central trapping wires.

the center of the trapping wires was removed using an RIE etch, as shown in Fig. 5b. Wire height is  $1.5 \,\mu\mathrm{m}$  and polyimide thickness is  $3.3 \,\mu\mathrm{m}$ . Figure 5a shows a stylus profilometer scan of the polyimide surface above the five wires. Around the center wire, the peak-to-peak height variation of the polyimide surface is 240 nm., giving a DOP of 85%.

The average grain size of a deposited film increases with the film thickness and the substrate temperature during deposition [21]. Cr/Au films were grown on polyimide surfaces at various thicknesses to observe the effect on grain size. The temperature of the substrates was controlled by water-cooling the substrate mount. The average grain diameter increased from 40 nm for a 100 nm film to 60 nm for a 1.5  $\mu$ m film. Magnetic field noise caused by thermally induced stray currents increases with film thickness – favoring thin shield layers [22].

Figure 6 shows an SEM image of the surface of the shield layer. Average grain size is determined using a counting method, with three smaller areas sampled from the image. The average diameter of the grains is calculated by dividing the image area by the number of grains counted, with the approximation that they are circular. The average grain diameter is 40 nm.

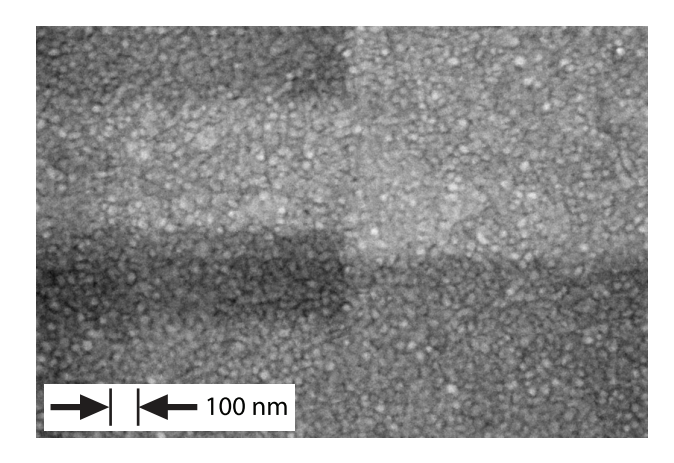


FIG. 6. SEM image of the surface of the shield layer.

### V. DISCUSSION

We have fabricated an atom chip for Rydberg atommetal surface interaction studies. The chip uses five parallel current-carrying wires  $(1.5 \,\mu\mathrm{m})$  thick Au) over a 20 nm Ti adhesion layer, and a 50 nm Pd buffer layer. The Pd is used to eliminate the diffusion of Ti into the Au during subsequent thermal processing. Wires are grown by thermal deposition and patterned using lift-off photolithography. The chip is planarized using three layers of polyimide PI 2562 with a full cure after each layer application. Polyimide is etched using RIE with a sputtered Al etch mask. To avoid etching pinholes through the polyimide, the polyimide is patterned in two stages: once after applying the first two layers and again after the third. A total thickness of  $3.3 \,\mu\mathrm{m}$  gives a degree of planarization of 85 %. The chip uses a Au electrostatic shield layer above the polyimide to isolate the Rydberg atoms from electric fields caused by potential differences between the trapping wires. This layer is also a reflective surface for the laser cooling beams and the surface with which the Rydberg atoms interact. The shield is fabricated by thermal deposition and lift-off photolithography. The Au grains of the shield are 40 nm in diameter, as measured using SEM images.

Despite their fundamental importance in a variety of experiments, surprisingly little has been done to systematically characterize the patch electric fields which exist over polycrystalline surfaces. As determined in Appendix C, patch fields should be detectable as far as  $100~\mu \mathrm{m}$  from our shield layer. A careful study of these fields should be of use in the design of experiments involving Rydberg atoms near surfaces [23–25].

We thank Dr. R. Mansour for the use of the CIRFE facility, and R. Al-Dahleh, B. Jolley and Dr. Czang-Ho Lee for their assistance. This work was supported by NSERC.

# Appendix A: Experimental System Incorporating Atom Chip

The atom chip is part of an experimental apparatus to study Rydberg atom surface interactions. In this appendix the entire system is described. Some of these steps have been demonstrated by our group using a preliminary (non-shielded) atom chip [26].

A vapor cell mirror MOT will cool and capture room temperature atoms of <sup>87</sup>Rb. After optical molasses and optical pumping, cold atoms will be trapped using a macroscopic Ioffe-Pritchard trap. The cloud of atoms will then be compressed and evaporatively cooled in this trap before transfer to the atom chip.

As far as the MOT and magnetic trapping is concerned, our approach is conventional, following existing designs in the literature [27, 28]. A U-shaped copper wire is embedded in the Macor beneath the chip and is used in conjunction with a pair of Helmholtz coils to form a magnetic quadrupole for a mirror MOT [9]. After a sufficient number of atoms have accumulated in the MOT, the cooling lasers are switched off, and an optical pumping beam is introduced to transfer most of the population to the F=2,  $m_F=2$  weak-field seeking state. They are then captured by an intermediate magnetic trap formed by a mm-sized Z-shaped wire (also embedded beneath the chip) and external coils. The lasers are switched off, leaving a purely magnetic trap. Then the atoms are evaporatively cooled using rf radiation while compressing the trap. The cold atoms that remain are transferred to the chip by ramping down the current in the Z-wire and increasing the currents in the atom chip wires. Once the atoms have been loaded into the atom chip trap, they can be positioned within a few  $\mu m$  of the chip surface and optically excited to Rydberg states.

Excitation into Rydberg states can be detected by applying an electric field pulse, which will ionize the atoms, and draw the resulting ions or electrons away from the surface towards a charged particle detector. By varying the Rydberg excitation frequency, spectra may be obtained. As discussed in Appendix C, the broadening of these spectra will be used to measure patch field distributions.

## Appendix B: Control of atom surface distance

The chip is suitable for confining cold clouds of atoms at distances ranging from  $2\,\mu\mathrm{m}$  to  $200\,\mu\mathrm{m}$  from the surface. The inner pair of U-wires and the center wire are used to trap the atoms at distances of less than  $50\,\mu\mathrm{m}$  from the surface. The outer pair of U-wires and the center wire are used for larger atom-surface distances.

Two effects contribute to uncertainty in the atomsurface distance. The cloud of atoms will have a finite size, so that not all atoms are the same distance from the surface. Any roughness in the surface (such as lessthan-perfect planarization over the trapping wires) will

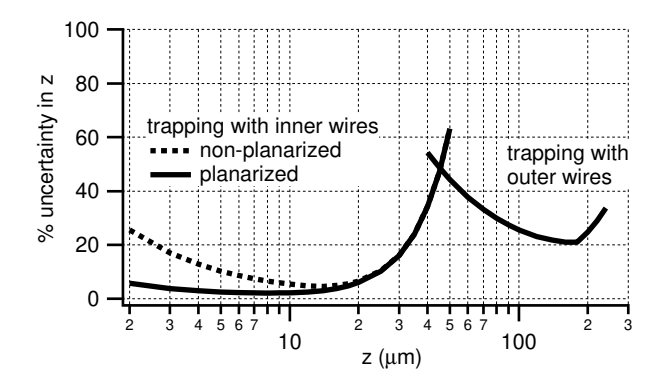


FIG. 7. Uncertainty in atom-surface distance z as a function of atom-surface distance for a 10  $\mu \rm K$  cloud (see text for details).

also cause variation in the atom-surface distance. The trapping parameters at various distances were calculated, assuming  $1 \, \mu \text{m}$  thick wires, maximum current density of  $3.5 \times 10^6 \,\mathrm{A/cm^2}$ , and an applied axial "Ioffe-Pritchard" field of 2 G, large enough to ensure that a 10  $\mu$ K cloud is completely within the harmonic regime of the trap. The uncertainty in the atom-surface distance due to the finite size of a  $10 \,\mu\text{K}$  atom cloud alone was calculated, taking the cloud size to be defined by the classical turning point of an atom with average kinetic energy. The uncertainty due to surface corrugations of  $1 \,\mu\mathrm{m}$  in height was added in quadrature. Plots of the uncertainty in atom-surface distance as a function of distance are shown in Fig. 7. For all distances considered, treating the  $10 \,\mu\mathrm{K}$  cloud as a classical thermal cloud is appropriate. Surface corrugations are the dominant source of uncertainty at short distances, and the finite cloud size dominates at long distances, where the confinement of the trap is much weaker.

At large (> 50  $\mu$ m) atom-surface distances, a 10  $\mu$ K cloud is undesirably large due to the weak confinement. However, the cloud can easily be made smaller with additional rf evaporative cooling to lower the temperature. The size of a thermal cloud in a harmonic potential scales as  $\sqrt{T}$ , so lowering the temperature of the cloud to 1  $\mu$ K would reduce the cloud size by slightly more than a factor of three.

As the cloud is moved toward the chip, the confinement strength increases, so the cloud is adiabatically compressed and heated. However, this heating can be compensated with additional rf evaporative cooling as long as enough atoms remain for good signal-to-noise in the Rydberg atom experiment.

# Appendix C: Patch electric fields and their detection using Rydberg atoms

Adsorbates cause inhomogeneous electric fields above surfaces [8, 29]. However, even in the absence of contaminants, a polycrystalline metal surface will exhibit significant inhomogeneous electric fields at distances from

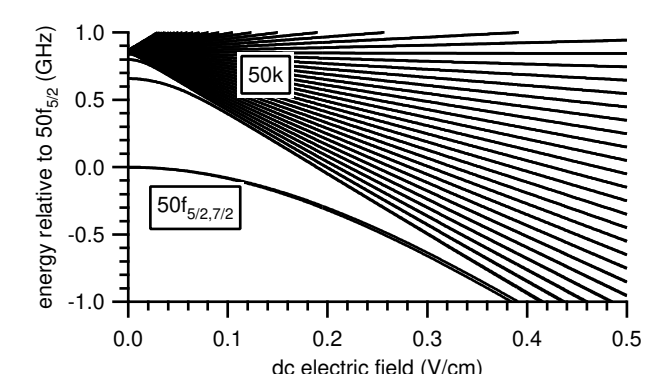


FIG. 8. Stark map of  $m_j = 1/2$  states near  $50f_{5/2,7/2}$  calculated using the procedures of Zimmerman *et al.* [37], with zero-field spectroscopic data from Ref. [38].

the surface extending far beyond the atomic scale [30]. These fields are due to the differences in work function between different crystal faces. To estimate the size of these fields, we have extended a simple model introduced by Rzchowski and Henderson [31]. The root-mean-square (RMS) value of the electric field is found to be [32]:

$$E_{rms} = \langle E^2 \rangle^{1/2} \approx 0.3 \left(\frac{\Phi_{rms}}{w}\right) \left(\frac{w}{z}\right)^2$$
 (C1)

for  $z \gg w$ , where  $w \times w$  is the average patch area, and  $\Phi_{rms}$  is the patch to patch variation in work function (away from the mean). For gold,  $\Phi_{rms} \approx 0.1 \,\mathrm{V}$  [33]. With  $w = 40 \,\mathrm{nm}$  for our fabricated gold shield layer, we expect  $E_{rms} = 1.3 \,\mathrm{mV/cm}$  at  $100 \,\mu\mathrm{m}$  from the surface.

For concreteness, we will consider the sensing of these patch fields using the  $5d_{5/2} \rightarrow 50f_{7/2}$  transition in Rb. There are several reasons for this choice: The complete excitation sequence  $5s \rightarrow 5p \rightarrow 5d \rightarrow 50f$  has been demonstrated previously [34, 35]. The three wavelengths involved (780, 776 and 1259 nm) are all available from relatively inexpensive external cavity diode laser systems, and are much longer than those required for the  $5s \rightarrow 5p \rightarrow ns$ ,  $5s \rightarrow 5p \rightarrow nd$ , or  $5s \rightarrow 5p$  excitation schemes – reducing photoelectron emission from the surface. (The work function of gold can be significantly lowered by adsorption of alkalis; see, for example, Ref. [36].) In addition, compared to the ns, np and nd series, the nf Rydberg states have significantly higher polarizabilities.

A Stark map showing the shift of the 50f states with electric field is shown in Fig. 8. Due to the quadratic nature of the low field shift it is desirable to apply a "bias" field to increase spectral sensitivity to electric field. This, however, should not be so large that the oscillator strength of the nd-nf transition is "diluted" by the manifold (the nk states in Fig. 8, adiabatically connected to states of  $\ell>3$ ). Dilution will reduce the signal level, degrading the signal-to-noise (S/N). In a field of  $0.2\,\mathrm{V/cm}$ , the state adiabatically connected with  $50\,f_{7/2}$ , shows an electric field sensitivity of  $-2.95\,\mathrm{GHz/(V/cm)}$ . Its total f character is 60%, and thus, should still be relatively straightforward to excite.

There will be contributions to the width of the  $5d_{5/2} - 50f_{7/2}$  line from the finite lifetime of the 5d state (600 kHz [39]), and the excitation laser linewidth. With a relatively straightfoward frequency stabilization scheme, we could expect a total linewidth of roughly 1 MHz.

To avoid Zeeman broadening due to the inhomogeneous magnetic microtrap fields, it will be necessary to turn these off shortly prior to Rydberg state excitation.

If we assume a S/N ratio sufficient to observe an additional 1 MHz of broadening, we will be sensitive to fields larger than 1 MHz /[2.95 GHz/(V/cm)]  $\approx 0.3\,\mathrm{mV/cm}$ . Thus, at  $100\,\mu\mathrm{m}$  from the shield, the patch fields ( $E_{rms}=1.3\,\mathrm{mV/cm}$ ) should be observable. As  $E_{rms}$  scales like  $1/z^2$ , the patch fields at smaller distances should be observable; although it may be desirable to use a less sensitive, lower-n Rydberg state closer to the surface to avoid spectral confusion.

Rydberg atoms near metal surfaces show an energy shift due to a dipole-dipole interaction with their electrostatic images (the Lennard-Jones shift [40]). This shift is split due to magnetic sublevel structure, and contributes to broadening due to the variation in atom-surface distance discussed in Appendix B. Therefore, to sense the patch fields, the Lennard Jones shift should be less than the broadening due to the patch fields. Using the formulae of Ref. [40] we estimate the Lennard-Jones shift of the  $50f_{7/2}$   $m_j = 1/2$  state – the axis of quantization is the surface normal – at  $z = 100 \,\mu\mathrm{m}$  to be 1.4 kHz. (This is probably an overestimate, as it assumes a perfectly conducting surface.) This shift scales like  $n^4/z^3$ [3] – at 10  $\mu$ m it is 1.4 MHz. However, this is still much smaller than the expected Stark broadening due to patch fields. A combination of zero average dc field, together with low z and n is best for enhancing the Lennard-Jones shift relative to Stark broadening [3].

T. F. Gallagher, Rydberg Atoms (Cambridge University Press, Cambridge, 1994).

<sup>[2]</sup> A. V. Chaplik, Soviet Physics JETP 27, 178 (1968).

<sup>[3]</sup> V. Sandoghdar, C. I. Sukenik, E. A. Hinds, and S. Haroche, Phys. Rev. Lett. 68, 3432 (1992).

<sup>[4]</sup> S. B. Hill, C. B. Haich, Z. Zhou, P. Nordlander, and F. B. Dunning, Phys. Rev. Lett. 85, 5444 (2000).

<sup>[5]</sup> R. Folman, P. Krüger, J. Schmiedmayer, J. Denschlag, and C. Henkel, Adv. At. Mol. Opt. Phys. 48, 263 (2002).

<sup>[6]</sup> J. Fortágh and C. Zimmerman, Rev. Mod. Phys. 79, 235 (2007).

<sup>[7]</sup> Y.-J. Lin, I. Teper, C. Chin, and V. Vuletić, Phys. Rev. Lett. 92, 050404 (2004).

<sup>[8]</sup> A. Tauschinsky, R. M. T. Thijssen, S. Whitlock, H. B.

- van Linden van den Heuvell, and R. J. C. Spreeuw, Phys. Rev. A 81, 063411 (2010).
- [9] J. Reichel, W. Hänsel, and T. Hänsch, Phys. Rev. Lett. 83, 3398 (1999).
- [10] J. Reichel, W. Hänsel, Hommelhoff, and T. Hänsch, Appl. Phys. B 72, 81 (2001).
- [11] B. Lev, Magnetic microtraps for cavity QED, Bose-Einstein condensates, and atom optics, Ph.D. thesis, California Institute of Technology (2006).
- [12] P. Treutlein, T. Hänsch, J. Reichel, A. Negretti, M. Cirone, and T. Calarco, Phys. Rev. A 74, 022312 (2006).
- [13] T. Nirrengarten, A. Qarry, C. Roux, A. Emmert, G. Nogues, M. Brune, J.-M. Raimond, and S. Haroche, Phys. Rev. Lett. 97, 200405 (2006).
- [14] J. Estève, C. Aussibal, T. Schumm, C. Figl, D. Mailly, I. Bouchoule, C. Westbrook, and A. Aspect, Phys. Rev. A 70, 043629 (2004).
- [15] S. Groth, P. Krüger, S. Wildermuth, R. Folman, T. Fernholz, and J. Schmiedmayer, Appl. Phys. Lett. 85, 2980 (2004).
- [16] W. Kern and D. Puotinen, RCA Rev., 187 (1970).
- [17] AZ nLOF 2000 Photoresist Data Sheet, Clariant-AZ Electronic Materials (2007).
- [18] P. Madakson, J. Appl. Phys. **79**, 1380 (1991).
- [19] A. Munitz and Y. Komem, Thin Solid Films 37, 171 (1976).
- [20] J. Pan, M. Pafchek, F. Judd, and J. Baxter (IEEE/SEMI International Electronics Manufacturing Technology Symposium, 2004).
- [21] Z. Liu, N. Brown, and A. McKinley, J. Phys. Cond. Matt. 9, 59 (1997).
- [22] B. Zhang, C. Henkel, E. Haller, S. Wildermuth, S. Hofferberth, P. Krüger, and J. Schmiedmayer, Eur. Phys. J. D 35, 97 (2005).
- [23] A. S. Sørensen, C. H. van der Wal, L. I. Childress, and M. D. Lukin, Phys. Rev. Lett. 92, 063601 (2004).

- [24] P. Hyafil, J. Mozley, A. Perrin, J. Tailleur, G. Nogues, M. Brune, J.-M. Raimond, and S. Haroche, Phys. Rev. Lett. 93, 103001 (2004).
- [25] I. Lesanovsky and P. Schmelcher, Phys. Rev. Lett. 95, 53001 (2005).
- [26] O. Cherry, J. D. Carter, and J. D. D. Martin, Can. J. Phys. 87, 633 (2009).
- [27] A. Kasper, S. Schneider, C. vom Hagen, M. Bartenstein, B. Engeser, T. Schumm, I. Bar-Joseph, R. Folman, L. Feenstra, and J. Schmiedmayer, J. Opt. B: Quant. Semiclass. Opt 85, 2980 (2004).
- [28] S. Wildermuth, P. Krüger, C. Becker, M. Brajdic, S. Haupt, A. Kasper, R. Folman, and J. Schmiedmayer, Phys. Rev. A 69, 030901 (2004).
- [29] J. M. Obrecht, R. J. Wild, and E. A. Cornell, Phys. Rev. A 75, 062903 (2007).
- [30] C. Herring and M. H. Nichols, Rev. Mod. Phys. 21, 185 (1949).
- [31] M. S. Rzchowski and J. R. Henderson, Phys. Rev. A 38, 4622 (1988).
- [32] J. D. Carter and J. D. D. Martin, Phys. Rev. A 83, 032902 (2011).
- [33] C. R. Lide, ed., CRC Handbook of Chemistry and Physics, 82nd ed. (CRC Press, Boca Raton, FL, 2001).
- [34] P. Filipovicz, P. Meystre, G. Rempe, and H. Walther, Opt. Acta 32, 1105 (1985).
- [35] P. Nussenzveig, F. Bernardot, M. Brune, J. Hare, J. M. Raimond, S. Haroche, and W. Gawlik, Phys. Rev. A 48, 3991 (1993).
- [36] D. F. Gray, Z. Zheng, K. A. Smith, and F. B. Dunning, Phys. Rev. A 38, 1601 (1988).
- [37] M. L. Zimmerman, M. G. Littman, M. M. Kash, and D. Kleppner, Phys. Rev. A 20, 2251 (1979).
- [38] J. Han, Y. Jamil, D. V. L. Norum, P. J. Tanner, and T. F. Gallagher, Phys. Rev. A 74, 054502 (2006).
- [39] A. Lindgard and S. E. Nielsen, Atomic Data and Nuclear Data Tables 19, 533 (1977).
- [40] E. A. Hinds, Adv. Atom. Mol. Phys. 28, 237 (1991).